Biochemistry

Article

Cite This: *Biochemistry* 2018, 57, 5672−5682

pubs.acs.org/biochemistry

Control of Hexamerization, Assembly, and Excluded Strand Specificity for the *Sulfolobus solfataricus* MCM Helicase

Brian W. Graham,[†,#] Michael E. Bougoulias,[‡] Katie L. Dodge,[‡] Carly T. Thaxton,[‡] Danae Olaso,[‡] Yeqing Tao,[§] Nicolas L. Young,[∥] Alan G. Marshall,[§,⊥] and Michael A. Trakselis*[,‡]

[†]Department of Chemistry, University of Pittsburgh, Pittsburgh, Pennsylvania 15260, United States

[‡]Department of Chemistry and Biochemistry, Baylor University, Waco, Texas 76798, United States

[§]Department of Chemistry, Florida State University, Tallahassee, Florida 32306, United States

[∥]Verna & Marrs McLean Department of Biochemistry & Molecular Biology, Baylor College of Medicine, One Baylor Plaza, Houston, Texas 77030-3411, United States

[⊥]National High Magnetic Field Laboratory, 1800 East Paul Dirac Drive, Tallahassee, Florida 32310, United States

Supporting Information

ABSTRACT: A growing body of evidence supports a steric exclusion and wrapping model for DNA unwinding in which hexameric helicases interact with the excluded single-stranded DNA (ssDNA) in addition to the encircled strand. Interactions with the excluded ssDNA have been shown to be mediated primarily by electrostatic interactions, but base stacking with surface-exposed tyrosine residues is an alternative hypothesis. Here, we mutated several external tyrosine and positively charged residues from full-length *Sulfolobus solfataricus* MCM along the proposed path of excluded strand binding and assessed their impact on DNA unwinding. Four of the five tyrosine residues had significant decreases in their level of unwinding, and one, Y519A, located within the $\alpha/\beta-\alpha$ linker region of the C-terminal domain, had the most severe perturbation attributed to the disruption of hexamerization. The Y519 mutant exhibits an enhanced and stabilized secondary structure that is modulated by temperature, binding DNA with a higher apparent affinity and suggesting a pathway for hexameric assembly. Hydrogen/deuterium exchange coupled to mass spectrometry was used to map deuterium uptake differences between wild-type and Y519A apo structures highlighting global differences in solvent accessible areas consistent with altered quaternary structure. Two of the five electrostatic mutants had significantly reduced levels of DNA unwinding and combined with previous mutations better define the exterior binding path. The importance of the electrostatic excluded strand interaction was confirmed by use of morpholino DNA substrates that showed analogous reduced unwinding rates. These results better define the hexameric assembly and influence of the excluded strand interactions in controlling DNA unwinding by the archaeal MCM complex.

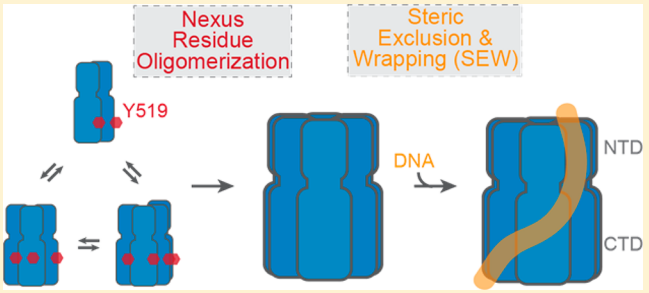

Hexameric DNA replication helicases are proposed to unwind duplex DNA by encircling and engaging one strand and excluding the other from the central channel through a steric exclusion (SE) mechanism. However, the role of the excluded strand in the molecular unwinding mechanism has generally been ignored. We have shown previously that the excluded strand interacts with the external surface and controls the unwinding efficiency for the *Sulfolobus solfataricus* minichromosome maintenance (*Sso*MCM) helicase.[2] The interaction of the external surface with the excluded single-stranded DNA (ssDNA) has been linked to various electrostatic residues along a putative binding path. This unwinding model in which hexameric helicases interact with both the encircled and excluded strands has been termed the steric exclusion and wrapping (SEW) model and can now be expanded to include the analogous hexameric DNA replication helicases in *Escherichia coli*, DnaB,[3] in addition to archaeal MCM. It is interesting to note that *Ec*DnaB has an opposite 5′ → 3′ translocation polarity and little sequence homology with MCM helicases, indicating that the SEW mechanism is a structurally conserved and not family conserved feature for unwinding.

In addition to *Sso*MCM, *Methanothermobacter thermoautotrophicus* MCM (*Mth*MCM) and *Pyrococcus furiosus* MCM (*Pfu*MCM) have served as homohexameric model enzymes for structural and biochemical assays for the more complex but homologous heterohexameric MCM2−7 helicase in eukaryotes.[4−8] MCM helicases are essential for both DNA replication initiation and elongation and are known to interact with accessory proteins that control DNA loading during

Received: July 17, 2018
Revised: August 21, 2018
Published: September 10, 2018

DOI: 10.1021/acs.biochem.8b00766
Biochemistry 2018, 57, 5672−5682

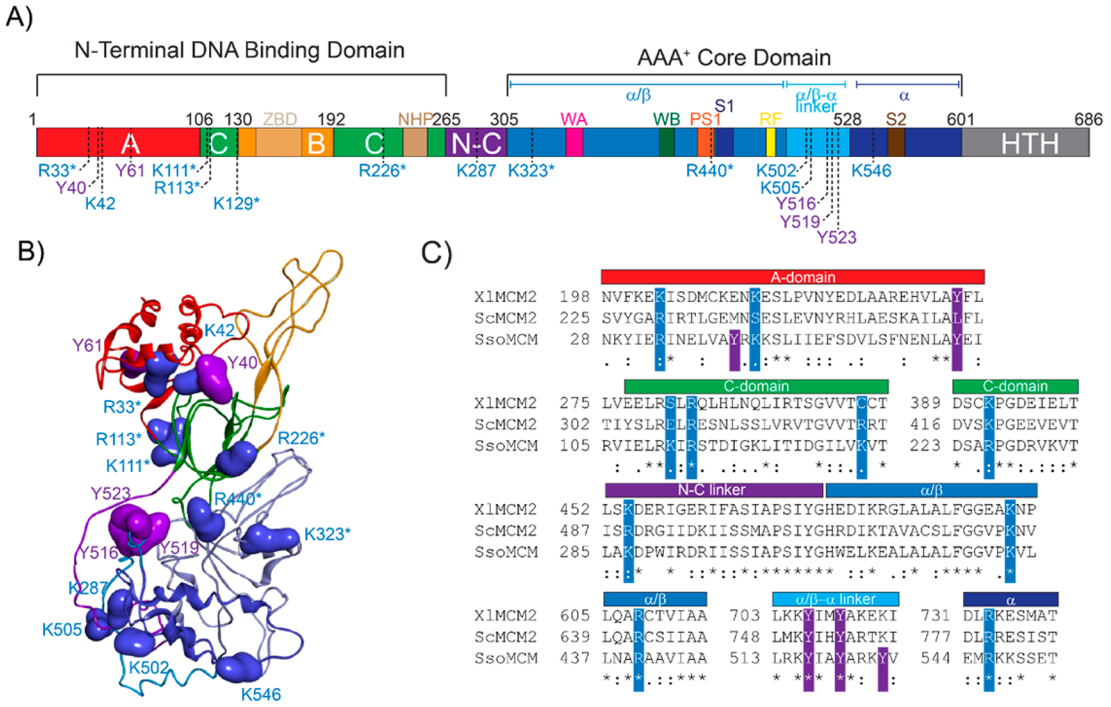

Figure 1. MCM domains, mutant locations, and sequence homology. (A) *Sso*MCM domain organization with the mutations indicated (asterisks denote data from previous reports).[1,2] Mutated residue positions are mapped onto (B) the tertiary structure (blue, electrostatic; purple, Tyr) and (C) the ClustalW2 alignment of *Hsa*MCM2, *Xla*MCM2, and *Sso*MCM in which *Hsa* indicates human, *Xla Xenopus laevis*, and *Sso S. solfataricus*.

initiation and unwinding rates during elongation. For example, *Sso*MCM interacts with both a GINS complex and a Cdc45 homologue (RecJ) that stimulate unwinding[9,10] and mimics the Cdc45−MCM−GINS (CMG) complex in eukaryotes.[11,12] Together, the archaeal MCM helicases have provided deep insight into the structural organization of the conserved motifs and domains and their contributions to DNA unwinding.

In addition to a monomeric near full-length crystal structure for *Sso*MCM,[13] other crystal structures of archaeal MCM have been determined as filaments,[14,15] from a hybrid hexamer with an N-terminal *Sso* domain and a C-terminal *Pfu* domain,[16] as well as numerous EM structures showing different conformations (hexamer, heptamer, and filament).[17−20] It is more than likely that various conformational states that include an open interface will contribute to MCM loading at origins of replication,[21] converting to the encircling of individual strands, interactions with accessory and loader proteins, and stimulating unwinding activity. The wealth of static structural data reveals the individual subdomains and motifs within an MCM monomer and provides important targets for biochemical analysis to better characterize these mechanisms.

The N-terminal domain (NTD) contains subdomains A−C and is connected by the N−C linker to the C-terminal domain (CTD) (Figure 1A). The A-subdomain imparts the snowflake-like appearance that may be able to exist in at least two conformations, compacted and extended;[13,16] the B-subdomain contains the Zn-binding motif, and the C-subdomain has one interior β-hairpin (NHP) that contacts the encircled strand.[17,22] The CTD contains an α/β-region that is connected to the α-region by the $\alpha/\beta-\alpha$ linker. The α/β-region has the characteristic AAA$^+$ motifs, including the Walker A and B sites, the arginine finger, and sensor 1 and 2 motifs.[23] The α-region consists of three α-helices that contain sensor 2 that packs against the α/β-region. The $\alpha/\beta-\alpha$ linker is 47 residues in length and is composed of two long α-helices connected by a loop sequence in a molecular handshake. It interlocks with the N−C linker connecting the NTD to the CTD and provides stability and connectivity throughout the monomer. The extreme C-terminus contains a flexible winged helix domain that may provide allosteric control of ATPase activity[24] and direct DNA engagement.

Here, we extend our examination of the exterior ssDNA binding path more completely by mutating several positively charged residues and testing potential effects of base-stacking tyrosine residues along the lateral length of *Sso*MCM. Two additional positively charged residues and four tyrosine residues were used to more completely define the exterior binding path on *Sso*MCM for the excluded strand. Altered morpholino DNA chemistry that eliminated the negatively charged backbone reduced the level of unwinding (analogous to the protein mutants), validating the importance of the excluded strand SEW interaction. It is interesting to note that a single tyrosine mutation (Y519A) was found to alter the secondary and tertiary structure and destabilize the quaternary hexameric state. An altered assembly mechanism for *Sso*MCM-(Y519A) shows that the wild type (WT) binds in a dimer-of-trimers mechanism to form a hexamer on fork DNA. In all, a nexus for hexamerization within the $\alpha/\beta-\alpha$ linker is identified, and the specific contributions of residues along the entire lateral length of *Sso*MCM that engage the excluded strand for efficient unwinding are defined.

EXPERIMENTAL PROCEDURES

Materials. ATP was obtained from Invitrogen (Carlsbad, CA). [γ-^{32}P]ATP was purchased from PerkinElmer (Waltham, MA). Optikinase was from USB Corp. (Cleveland, OH). All other materials were from commercial sources and were analytical grade or better. Helicase buffer is used in all

DOI: 10.1021/acs.biochem.8b00766
Biochemistry 2018, 57, 5672−5682

unwinding and binding reactions and consists of 125 mM potassium acetate, 25 mM Tris acetate (pH 7.5), and 10 mM magnesium acetate. DNA primers and substrates (Table S1) were all synthesized by IDT (Coralville, IA).

Cloning and Purification of *Sso*MCM Mutants. *Sso*MCM Y40A, K42A, Y61A, K287A, K502A/K505A, Y516A, Y519A, Y523A, K546A, and R560A were created by use of a standard QuikChange protocol (Agilent, Santa Clara, CA) with KAPA HiFi DNA polymerase (KAPA Biosystems, Woburn, MA). Mutations were initially confirmed by silent mutations to create unique restriction sites and then by the DNA sequencing facility at the University of Pittsburgh or the DNA Sequencing Faculty at The University of Texas at Austin (Austin, TX). The full-length WT and the point mutants were purified as previously described.[1,2] Briefly, autoinduced *Sso*MCM was heat-treated at 70 °C for 20 min, and the supernatant was applied to MonoQ, heparin, and S-200 gel filtration columns by use of AKTA Pure (GE Healthcare) to isolate the purified hexameric species.

Steady-State DNA Unwinding Assays. Unwinding assays were performed as previously described[1,2] in helicase buffer. *Sso*MCM variants (2.0 μM monomer and 400 nM hexamer) were incubated with 15 nM 5′-radiolabeled fork DNA (DNA14/DNA15) for 5 min at 60 °C, and reactions initiated with 2 mM ATP. Unwinding reactions were performed at 60 °C for the indicated times before being quenched with an equal volume of glycerol quench [1.6% (w/v) sodium dodecyl sulfate (SDS), 30% (v/v) glycerol, 0.1% (w/v) bromophenol blue, 100 mM EDTA (pH 8.0), and 150 nM trap ssDNA, identical to the labeled strand]. DNA was resolved on 20% acrylamide/1× TBE gels, phosphorimaged with a Storm 820 instrument (GE Healthsciences), and quantified in terms of the unwinding rate (fraction unwound per minute).

ATPase Assays. *Sso*MCM variants (2 μM) were incubated in the absence or presence of unlabeled forked DNA as previously described[22] in helicase buffer. Briefly, 30 μL reaction mixtures were incubated at 60 °C for 5 min, and 2 mM ATP (with tracer [γ-^{32}P]ATP) was added to initiate the reaction. Samples were quenched 5, 10, and 15 min after initiation in equal volumes of 0.7 M formic acid. A total of 0.8 μL of the quenched reaction mixture was spotted onto Millipore TLC PEI Cellulose F, allowed to dry, resolved in 0.6 M potassium phosphate (pH 3.5), phosphorimaged, and quantified in terms of the ATPase rate (picomoles per minute).

Analytical Gel Filtration Chromatography. Analytical gel filtration chromatography was performed as previously described.[25] Briefly, the analytical gel filtration column (Superdex 200 10/30) was calibrated with protein standards, including thyroglobulin (669 kDa), catalase (250 kDa), conalbumin (75 kDa), myoglobin (17.6 kDa), and vitamin B_{12} (1.2 kDa). *Sso*MCM variants containing ∼14 nmol of protein, supplemented with vitamin B_{12} as an internal standard, were applied to the column at a rate of 0.1 mL/min in a buffer containing 25 mM Tris-HCl (pH 7.5), 100 mM NaCl, and 5 mM β-mercaptoethanol.

Electrophoretic Mobility Shift Assays (EMSAs). EMSAs were performed as previously described.[26] *Sso*MCM variants were incubated with ^{32}P-labeled forked DNA in helicase buffer. Briefly, 10 μL reaction mixtures were incubated for 10 min at 60 °C to promote native thermodynamic complex formation, and 2 μL of loading buffer [30% (v/v) glycerol] was added prior to being resolved on 5% native polyacrylamide gels. The gels were incubated on a rocker in a fixing solution [70% (v/v) doubly deionized H_2O, 20% (v/v) methanol, and 10% (v/v) glacial acetic acid] for 20 min. The gels were then dried for 1 h and phosphorimaged. Four regions were quantified with ImageQuant version 5.0 (GE Healthcare): unbound DNA, hexamer (bound region at top of the gel), nonhexamer (bound region between the hexamer and unbound), and bound (nonhexamer and hexamer). Both bound and hexamer were fitted to the following equation:

$$Y = \frac{A[\mathrm{MCM}]^n}{K_d{}^n + [\mathrm{MCM}]^n} \quad (1)$$

where A is the amplitude, K_d is the dissociation constant for the specified species, and n is the Hill coefficient.

Circular Dichroism (CD) Spectroscopy. CD was performed as previously described.[27] Measurements were performed with an Olis (Bogart, GA) DSM17 CD spectrophotometer in 0.1 cm path-length quartz cuvettes; 300 μL reaction mixtures of *Sso*MCM variants (4 μM) were prepared in helicase buffer in the absence and presence of forked DNA (0.6 μM). Wavelength scans were collected at 20 °C from 200 to 260 nm with 5 s integration periods, a 1 nm step size, and a 2 nm bandwidth. Spectra were corrected for a buffer blank collected in the same cell and residual baseline molar ellipticity at 260 nm. The individual spectra were averaged and compared with the spectrum of their mixture [1:1 (v/v)]. The molar ellipticity (θ) was calculated with the following equation:

$$[\theta] = \frac{\theta_{\mathrm{samp}} - \theta_{\mathrm{blank}} - \theta_{\mathrm{avg}}}{10[\mathrm{M}] \times 0.1\ \mathrm{cm} \times \mathrm{no.\ of\ residues}} \times 10^{-3} \quad (2)$$

where Θ_{samp} and Θ_{blank} are the molar ellipticities for the sample and blank, respectively, and Θ_{avg} is the average molar ellipticity that is calculated from the following equation:

$$[\theta_{\mathrm{avg}}] = \theta_{255-260\mathrm{samp}} - \theta_{255-260\mathrm{blank}} \quad (3)$$

where 255−260 is the average molar ellipticity from 255 to 260 nm for either the sample or the blank and [M] is the concentration. Thermal denaturation experiments were performed by monitoring molar ellipticity at both 222 and 260 nm from 20 to 95 °C in 3 °C intervals with a 0.5 °C dead band, a 5 s averaging period, and a 2 min equilibration period at each temperature. The molar ellipticity was calculated similarly from the following equation:

$$[\theta] = \frac{\theta_{\mathrm{samp@222}} - \theta_{\mathrm{blank@222}} - \theta_{\mathrm{blank@260}}}{10[\mathrm{M}] \times 0.1\ \mathrm{cm} \times \mathrm{no.\ of\ residues}} \times 10^{-3} \quad (4)$$

where the molar ellipticities (θ) are monitored at either 222 or 260 nm for either the sample (samp) or buffer (blank). All parameters reported from CD measurements are the average of two or three independent experiments. Molar ellipticities (θ) were fitted by use of the updated version of K2D software, K2D2,[28−30] to estimate the percentage of α-helix and β-sheet character relative to reference data set CDDATA.43 from CDPRO.

Hydrogen/Deuterium Exchange Coupled to Mass Spectrometry (HDX-MS). Hydrogen/deuterium exchange (HDX) was performed as previously described.[1] Stock solutions of *Sso*MCM WT or Y519A (∼9 μM) were prepared in helicase buffer before being automatically diluted into D_2O for specified incubation periods before acid quench and

DOI: 10.1021/acs.biochem.8b00766
Biochemistry 2018, 57, 5672−5682

proteolysis. Online LC electrospray ionization of peptides was performed by use of a 14.5 T FT-ICR MS instrument with an LTQ Velos (Thermo Fisher Scientific, San Jose, CA) front end and analyzed with the Predator software package.[31] Deuterium uptake kinetics were calculated as previously described.[32] The average relative deuterium uptake difference (ARDD) between the free and complexed protein was calculated from the following equation:

$$\mathrm{ARDD} = \sum_i \frac{A(t_i) - B(t_i)}{A(t_i)} \quad (5)$$

where A and B are deuterium uptake for Y519A and WT, after specified incubation periods (t_i).[33]

Butterfly plots[34] were created to compare deuterium uptake for WT and Y519A based on the relative fraction deuterated for every peptide exhibiting a standard deviation of <0.5. The fraction deuterated from each peptide was assigned to each amino acid, and an average was then calculated. This average, for each incubation period, was then plotted as a relative fractional exchange versus amino acid residue number.

Single-Turnover DNA/Morpholino Unwinding Assays. Single-turnover helicase unwinding assays were assembled in helicase buffer. A 150 nM concentration of ^{32}P-radiolabeled forked DNA (as indicated) was incubated with 2 μM *Sso*MCM at 60 °C for 5 min before the reaction was initiated with 2 mM ATP and a 150 nM ssDNA trap (unlabeled strand with the same sequence as the radiolabeled strand). A 5′-^{32}P-labeled 53-base encircled strand (DNA162) was annealed to either an 18-base complementary DNA (DNA161) or morpholino (DNA160m) strand with a seven-base 5′ flap. Reactions were quenched with an equal volume of a quench solution [1.6% SDS, 50% glycerol, 0.1% (w/v) bromophenol blue, and 100 mM EDTA] and additional 150 nM ssDNA trap at various times. Reaction mixtures were placed on ice until loading and were resolved in 20% acrylamide/TBE gels. The gels were exposed to a phosphor screen overnight and imaged with a Storm 820 instrument (GE Healthcare, Sunnyvale, CA). The fraction unwound was calculated from the following equation:

$$F = \left[\frac{I_{s(t)}}{I_{s(t)} + I_{D(t)}} - \frac{I_{s(0)}}{I_{s(0)} + I_{D(0)}}\right] \Big/ \left[\frac{I_{s(b)}}{I_{s(b)} + I_{D(b)}} - \frac{I_{s(0)}}{I_{s(0)} + I_{D(0)}}\right] \quad (6)$$

where $I_{s(t)}$ and $I_{D(t)}$ are the intensities of the single- and double-strand bands at time t and subscripts 0 and b indicate equivalent counts at time zero and the boiled sample, respectively. The fraction unwound (per minute) was calculated from a linear regression fit of the fraction unwound as a function of time.

RESULTS

Creation of External Electrostatic or Base-Stacking Surface Mutants of *Sso*MCM. To more completely characterize the excluded ssDNA binding path on the exterior surface of *Sso*MCM, we created additional lysine, arginine, and tyrosine to alanine mutants. In addition to electrostatic interactions with the phosphate backbone, base-stacking interactions of external tyrosines can stabilize DNA bases. Using the *Sso*MCM crystal structure,[13] we identified five additional potential electrostatic sites (K42, R91, K287, K502/K505, and K546) and five external surface tyrosine residues (Y40, Y61, Y516, Y519, and Y523) along the proposed binding path.[1] R91, K502, and K505 are surface-exposed, but others form potential exterior salt bridges, including K42:E36, K546:E584, and K546:E542 salt bridges. In addition to external electrostatic mutations that we have already tested,[1,2] these additional residues span the linear amino acid sequence (including the untested $\alpha/\beta-\alpha$ linker) and the lateral length of the *Sso*MCM structure (Figure 1A–C). R91, K287, K502/K505, and K546 are part of peptides with reduced deuteration uptake kinetics when DNA is included,[1] whereas K42 acts as a control. All electrostatic mutation sites are conserved among eukaryotes (Figure 1C).

The tyrosines are located either in the A subdomain or in the $\alpha/\beta-\alpha$ linker region (Figure 1A–C), and these two regions were identified previously as probable external binding sites for ssDNA.[1] Y40, Y61, and Y523 are free on the surface; however, Y516 (OH) is H-bonded to the carbonyl amide of D270, and Y519 is partially buried. Y40, Y516, and Y523 are contained in peptides with reduced deuteration uptake kinetics when fork DNA is included, whereas Y61 and Y519 act as controls. Y61, Y516, and Y519 are conserved among eukaryotes, whereas Y40 and Y523 are not (Figure 1C).

WT *Sso*MCM is known to form a hexamer in solution even in the absence of DNA and ATP.[22,35] To characterize the oligomeric state of all of the mutants (Figure 2A), analytical gel filtration chromatography was used (Figure 2B). The molecular weights of the standards and the corresponding elution profiles for each mutant compared to that of WT are shown. The molecular weight of the *Sso*MCM monomer is 77.4 kDa, whereas that of the homohexamer is 464.4 kDa. WT and all point mutants except for Y519A elute similarly, indicating hexameric species. Y519A has three unresolved peaks eluting after the hexameric size that likely correspond to a majority dimer and lesser trimer, and tetramer species indicating a less stable complex. Anecdotally, purification of Y519A was more challenging with an increased level of precipitation and a persistent minor contaminant that potentially correlates with the size of the molecular chaperone, GroEL.

Both Electrostatics and Base Stacking Contribute to the Excluded Strand Interaction Path. We first tested the DNA unwinding ability of each of the mutants on fork DNA (Figure 3A,B). R91A, K287A, and all of the Tyr mutants had significantly reduced DNA unwinding rates compared to that of the WT. We note that K546A had unwinding rates consistently greater than those of the WT, but not significantly so. The sensor-2 mutant (R560A)[23] was used as a negative control for unwinding and ATPase activity. Comparing previous unwinding rates of additional *Sso*MCM mutants (dagger in Figure 3B) provides a clearer picture of the impact of external site mutations on DNA unwinding.

We have previously characterized the ATP hydrolysis rate of *Sso*MCM in the absence and presence of DNA.[22,26] In the presence of DNA, *Sso*MCM's ATPase rate is stimulated approximately 1.5-fold, correlating with unwinding activation or translocation. We measured the ATPase rate among mutants in the presence and absence of DNA using sensor-2 as a negative control (Figure 3C). All mutants had stimulated ATPase activity in the presence of DNA; however, only Y519A had significantly lower absolute ATPase activity compared to that of the WT, probably because of disruption of the

DOI: 10.1021/acs.biochem.8b00766
Biochemistry 2018, 57, 5672–5682

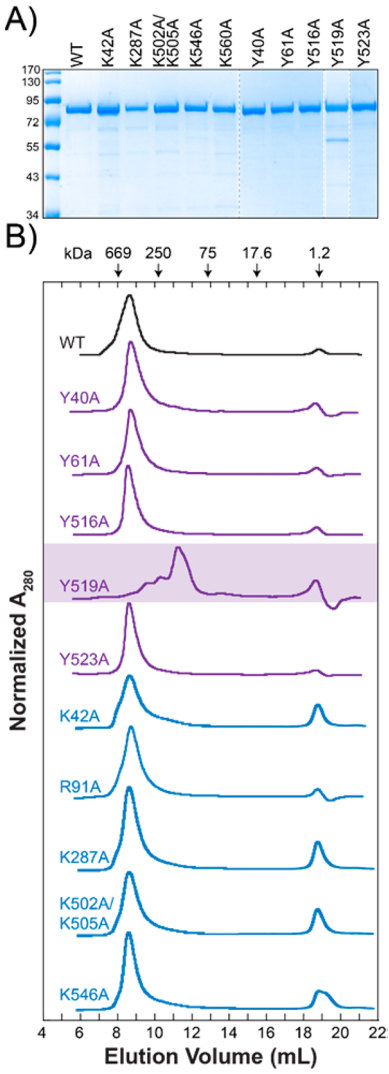

Figure 2. Purification of *Sso*MCM mutants and gel filtration profiles. (A) Coomassie-stained gel of purified *Sso*MCM variants. (B) Normalized A_{280} (mAu) vs elution volume for the SsoMCM variants analyzed by analytical gel filtration chromatography. Molecular weight standards (kilodaltons) are indicated at the top, corresponding to elution volumes. Vitamin B_{12} (1.2 kDa) was added to each sample to account for any drift during the run.

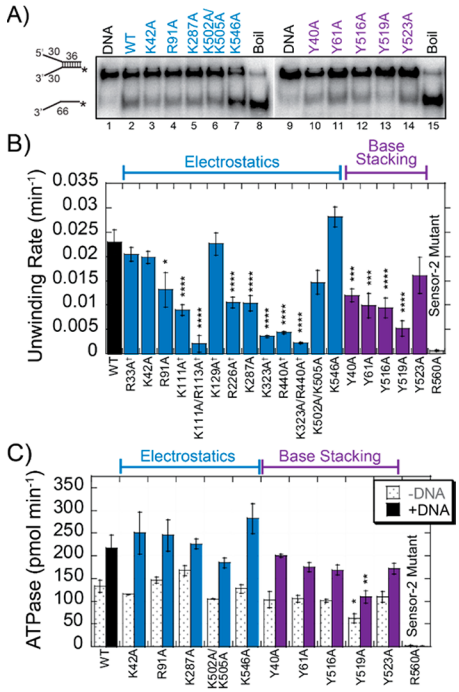

Figure 3. Enzymatic activity of the *Sso*MCM mutants. (A) ^{32}P-labeled fork DNA14/DNA15 unwinding by *Sso*MCM variants monitored in a 20% PAGE gel at a representative 15 min time point and phosphorimaged. (B) Quantification of the unwinding rate and significance for each mutant compared to the WT. A dagger denotes unwinding rates calculated previously for comparison.[1,2] Error bars represent the standard error from at least three independent time course unwinding experiments. (C) Calculated ATPase rate (for *Sso*MCM variants in the absence (dotted) and presence (solid) of DNA14/DNA15. Error bars represent the standard error from at least three independent time course ATPase experiments. *p* values (*<0.05, **<0.01, and ***<0.005) were calculated compared to the WT.

hexameric species that forms the ATPase active site *in trans* between adjacent subunits.[23] It is possible that the ATPase activity of Y519A is artificially enhanced by the copurifying minor contaminant, especially if it is GroEL, which has its own ATPase activity and is partially thermostable past 60 °C,[36] a temperature used in heat treatment during purification.

***Sso*MCM(Y519A) Has an Altered Stoichiometry That Affects Assembly on DNA.** We elected to further characterize the unique Y519A mutant, which is rare in its ability to singularly disrupt the hexameric species. We compared the unwinding kinetics for 2 μM WT and the slowest-unwinding mutant, Y519A, at different concentrations (Figure 4A,B). Titration of Y519A (1, 2, 4, and 8 μM) was performed to potentially promote hexamer formation to activate unwinding but did not significantly increase the unwinding kinetics. WT unwinds at a rate of 0.022 min^{-1}, whereas Y519A unwinds 3–4-fold slower (0.0067 min^{-1}). There is essentially no increase in rate with an increase in Y519A concentration, suggesting that the oligomeric state may be saturating in this concentration range. The ATP hydrolysis rate of Y519 increases linearly with concentration as expected but is always significantly lower than that for the WT (Figure S1).

To test any DNA binding differences between the WT and Y519A that may explain the altered oligomeric state, decreased level of unwinding, and decreased ATPase rates, we used EMSAs. EMSAs not only can quantify the binding affinity (K_d) of a protein for DNA but also can identify multiple oligomeric states bound to DNA. Both WT and Y519A *Sso*MCM were titrated into ^{32}P-labeled forked DNA (Figure 4D,E), and we quantified two fractional binding states: hexamer and total bound. We classified hexamer binding as the region near the top of the gel, whereas total bound is anything above free DNA. The hexameric species has entered the gel and is consistent with the migration noted previously.[8,22,26] For Y519A, there are also clear bands consistent with the dimer, trimer, and tetramer, enabling us to determine the position of a faint intermediate trimer band for the WT. Although these bands are visible on the gel, it is difficult to absolutely separate and quantify these fractional states; therefore, we only separately quantified the hexamer and total amount shifted.

Surprisingly, quantification of WT or Y519A hexamer binding is identical: 1.7 ± 0.2 or 1.6 ± 0.4 μM (Figure 4F). Quantification of the total bound independent of oligomeric state shows that Y519A binds DNA with a 2.4-fold greater affinity (0.20 ± 0.01 μM vs 0.49 ± 0.02 μM). Both binding

DOI: 10.1021/acs.biochem.8b00766
Biochemistry 2018, 57, 5672–5682

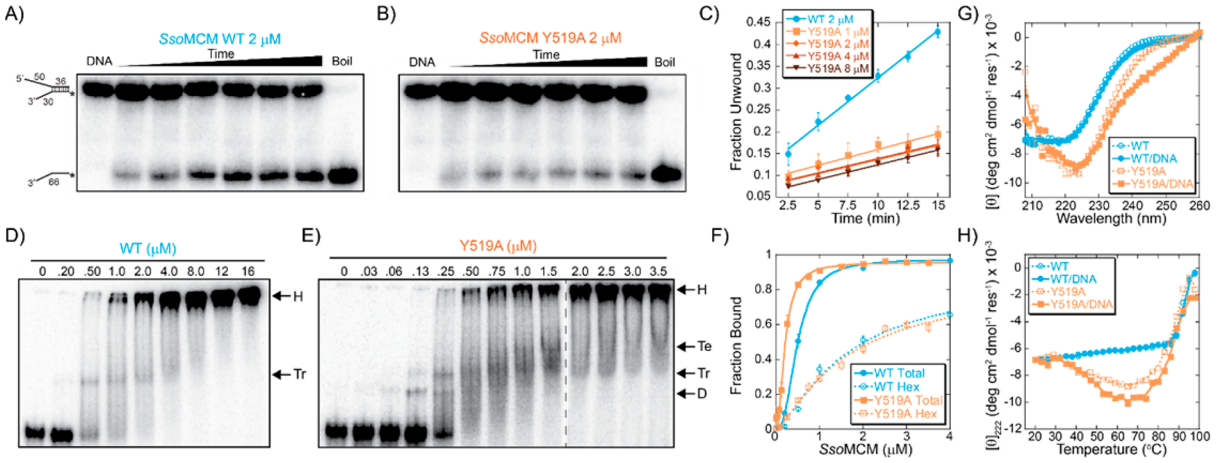

Figure 4. Biochemical characterization of *Sso*MCM(Y519A). Representative forked DNA unwinding by 2 mM *Sso*MCM (A) WT or (B) Y519A analyzed on a 14% PAGE gel over 15 min. (C) Quantification of the steady-state rate of fork unwinding by WT (2 μM) and Y519A (1, 2, 4, and 8 μM), fitted to a linear equation. Error bars represent the standard error from at least three independent unwinding experiments. Electrophoretic mobility shift assay (EMSA) of (D) WT or (E) Y519A *Sso*MCM binding to DNA titrated in the presence of 15 nM ^{32}P-labeled forked DNA. Indicated are approximate positions of the hexamer (H), tetramer (Te), trimer (Tr), and dimer (D). (F) Quantification of the total *Sso*MCM WT (cyan) and Y519A (orange) fraction bound (● or ■) or formation of hexamer (○ or □). The fitted K_d for total binding for the WT is 0.49 ± 0.02 μM (Hill coefficient of 2.5 ± 0.2) and for Y519A is 0.20 ± 0.01 μM (Hill coefficient of 2.0 ± 0.2). The fitted K_d for hexamer binding for the WT is 1.7 ± 0.2 μM and for Y519A is 1.6 ± 0.4 μM. (G) Molar ellipticity (degrees square centimeters per decimole per residue) × 10^{-3} vs wavelength (nanometers) in the absence (empty symbols) and presence of forked DNA (0.6 μM) (filled symbols) for the WT (cyan, ○ and ●) and Y519A (orange, □ and ■) *Sso*MCM (4 μM). (H) Molar ellipticity at 222 nm (degrees square centimeters per decimole per residue) × 10^{-3} vs temperature (degrees Celsius).

curves fitted with positive cooperativity, 2.5 ± 0.2 for the WT and 2.0 ± 0.2 for Y519A. The calculated value for WT binding is comparable to previous results acquired through fluorescence anisotropy (0.45 ± 0.08 μM),[2] but binding by Y519A is tighter than for any other *Sso*MCM variant tested. A comparison of the bound populations for WT versus Y519A at 0.5 μM most easily reveals this difference in binding affinity (Figure 4D, lane 3, and Figure 4E, lane 6). We attribute this increased affinity for DNA to a larger dimer/trimer/tetramer population equilibrium for Y519A that can more easily assemble onto DNA, as indicated by the dimer, trimer, and tetramer species on the gel. On the basis of these fractional bands, the measured affinities, and the Hill coefficients, we anticipate that WT *Sso*MCM would assemble on DNA initially as a trimer followed by nucleation to form the hexamer, whereas Y519A would initially assemble as a dimer followed by trimer, tetramer, and hexamer states, in addition to a dimer of trimers.

CD provides valuable information about the secondary structure of a protein. α-Helices (208 and 222 nm), β-sheets (218 nm), and random coils (198 nm) exhibit different molar ellipticity minima. We analyzed the far-ultraviolet CD spectrum for *Sso*MCM WT and Y519A, in the absence and presence of forked DNA (Figure 4G). The Y519A spectrum deviates to both higher wavelengths and a decreased overall molar ellipticity. We calculated and compared the relative α-helical and β-sheet fractions for WT (56.8 and 5.1%, respectively) and Y519A (>65 and 4.3%, respectively) from the measured molar ellipticity. The error is greater for Y519A because of a weaker fit to the reference CD data set, especially at lower wavelengths, but Y519A has clearly more α-helical character than does WT. On the basis of the available structural data for *Sso*MCM,[13,16,24] the percent α-helix is ∼36% and that of β-sheet is ∼17% (PsiPred).[37] The presence of DNA does not significantly change the secondary structure profile for the WT but does result in an altered spectrum (>235 nm) for Y519A. Analysis of this deviation (240−260 nm) is difficult because of insufficient analysis software for DNA−protein complexes but can be correlated with a change in the DNA conformation in addition to a further altered *Sso*MCM secondary structure.

To assess any differences in protein stability and/or structure for WT *Sso*MCM versus Y519A, temperature-dependent CD experiments (at 222 nm) were performed in the absence and presence of DNA (Figure 4H). DNA does not appear to increase stability or change the profile significantly for WT *Sso*MCM. However, addition of DNA to Y519A slightly shifts the melting temperature (T_m). Y519A by itself displays an interesting thermal melting profile in which increasing the temperature toward a physiological range for *Sulfolobus* (∼70−75 °C) appears to enhance secondary structure (decreased ellipticity at 222 nm, with a minimum at 66 °C), primarily α-helix, prior to melting at a T_m slightly greater than that of the WT. In all cases, the actual T_m is difficult to calculate directly, because full denaturation occurs above 100 °C, and our ellipticity profile is not saturating. Nevertheless, it is clear that Y519 has thermally induced formation of α-helical character (∼50−80 °C), which stabilizes the secondary structure relative to that of WT *Sso*MCM.

HDX-MS Shows Global Destabilization and More Exposed Surface Area for *Sso*MCM(Y519A). To validate the quaternary structure changes of Y519A relative to WT *Sso*MCM, we used HDX-MS to determine peptide regions of significant deuterium uptake differences that could correlate with the altered structure of Y519A. We have used HDX-MS previously to validate the hexameric model of *Sso*MCM and determine the external binding sites for the excluded strand to validate the SEW model.[1] We compared the deuterium uptake profiles for WT relative to Y519A in the absence of DNA and found many significant regions with altered kinetics (Figure

DOI: 10.1021/acs.biochem.8b00766
Biochemistry 2018, 57, 5672−5682

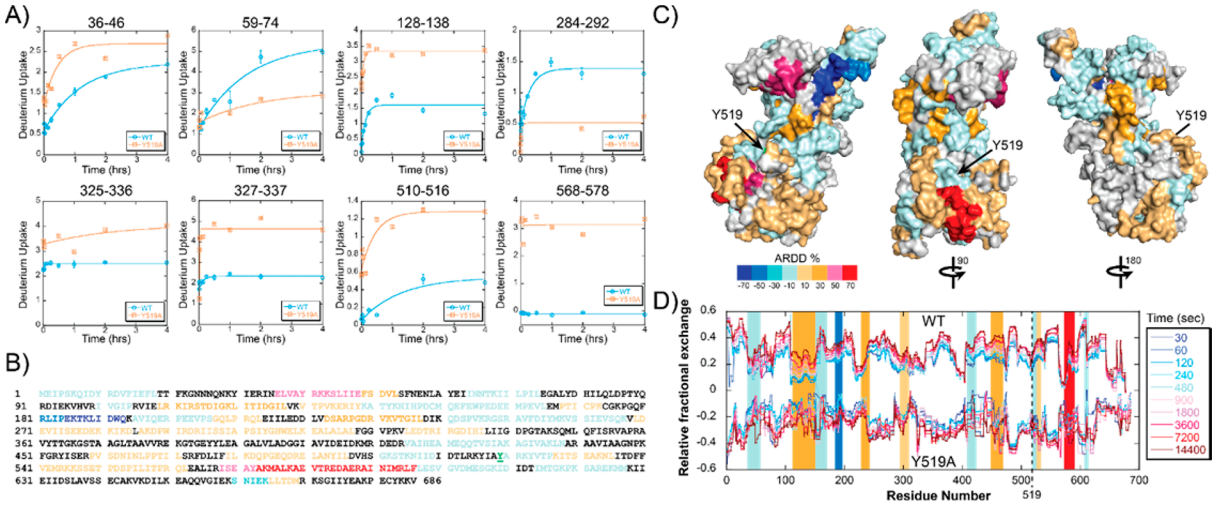

Figure 5. HDX uptake profiles for WT *Sso*MCM and Y519A. (A) Deuterium incorporation during the H/D exchange period for representative peptides, showing differences between the two conditions. Average relative deuterium uptake difference (ARDD) percent difference color coding for (B) the primary sequence of *Sso*MCM (Y519 is underlined and colored green) and (C) peptide regions with significant ARDD percent differences (Y519A minus WT) color-mapped onto the surface of the *Sso*MCM monomer. (D) HDX butterfly plots for WT *Sso*MCM (positive values) vs Y519A (negative values) showing relative fractional exchange as a function of amino acid residue number. Lines are color-coded from shades of blue to red from the 30 to 14400 s deuterium exchange period. Y519A is indicated by a dashed line. Shaded regions correspond to significant changes in relative fractional change kinetics correlated with ARDD colors.

5A). Not surprisingly, there is generally more rapid deuterium uptake for Y519A within the CTD around the region where Y519 is located. In particular, peptides 325−336, 327−337, 510−516, and 568−578 all show increased rates of deuterium uptake for Y519A.

We calculated the average relative deuterium uptake differences (ARDD%) between the WT and Y519A and mapped the percentages onto the primary sequence (Figure 5B) or monomer structure of *Sso*MCM (Figure 5C). Some of the largest increases occur within the α-region in the AAA$^+$ core domain (i.e., 568−596) and within the N−C linker, both of which are situated just adjacent to where Y519 resides. Other complex changes (both increases and decreases) in the rate of deuterium uptake are noted in the NTD. A butterfly plot representation of the relative fractional exchange averaged for each amino acid highlights global deuterium uptake differences between the WT and Y519A (Figure 5D). Generally, changes in deuterium uptake profiles can be seen throughout the entire protein sequence. More specifically in addition to changes noted in the CTD, increases in the level of deuteration are noted in peptides containing residues 36−48, and decreases for residues 140−166 and 181−193, all within the A-subdomain in the NTD. The A-subdomain seems to be the most labile of all domains and motifs, because it has adopted various conformations in the available structures of archaeal MCM.[13,15,16] It is important to note that small changes in the $\alpha/\beta-\alpha$ linker (i.e., Y519A) have profound consequences for the overall protein structure of *Sso*MCM that propagate from the CTD up through and into the NTD.

Altered Electrostatics on the Excluded Strand Reduce the Rate of DNA Unwinding by WT *Sso*MCM. To validate whether the affected electrostatic mutants (Figure 3) have reduced rates of unwinding because of a perturbation of the interaction with the excluded strand, we performed DNA unwinding reactions with a 5′-morpholino (morph) strand and WT *Sso*MCM. Morpholino nucleic acids utilize morpholine rings and phosphorodiamidate linkages that eliminate negative charges but retain native base pairing properties that are as stable or more stable than those of an equivalent DNA duplex.[38,39] Previously, the analogous 5′ → 3′ hexameric T7 gp4 and *E. coli* DnaB DNA helicases were shown to unwind excluded strand morpholino substrates with a rate and efficiency greater than those for DNA.[3,40] This enhanced unwinding activity was attributed to the disruption of the helicase's interaction with the displaced strand that limits its activity.

It is interesting that *Sso*MCM unwinds excluded strand morpholino substrates with a profoundly reduced rate compared to that of a DNA/DNA duplex (Figure 6A,B). The single-turnover rate of unwinding for the Morph/DNA is 8-fold slower than for DNA/DNA (Figure 6C). This reduced rate of unwinding confirms the requirement for favorable electrostatic interactions with the excluded strand to facilitate unwinding. The use of single-turnover experiments also suggests that the excluded strand interaction provides more stability when bound to DNA to facilitate unwinding.

DISCUSSION

The exterior surface of *Sso*MCM has been shown to interact with the excluded ssDNA during unwinding primarily through electrostatic interactions with positively charged amino acids along the entire lateral length.[1,2] However, it is likely that additional residues are involved in stabilizing the excluded strand, including potential base-stacking amino acids such as the available surface tyrosines. Of the five additional electrostatic residues that were tested, only mutation at R91 and K287 significantly reduced the rate of DNA unwinding. Four of the five tyrosine mutations also significantly reduced the rate of DNA unwinding, highlighting the importance of recognizing and stabilizing the base in addition to the phosphate backbone. The selection of the mutations was based on identification from our previous HDX-MS experiments globally defining the external binding path.[1] The selection of mutations was further motivated by an interest in understanding the role of the $\alpha/\beta-\alpha$ linker connecting the two subdomains (α/β and α)

DOI: 10.1021/acs.biochem.8b00766
Biochemistry 2018, 57, 5672−5682

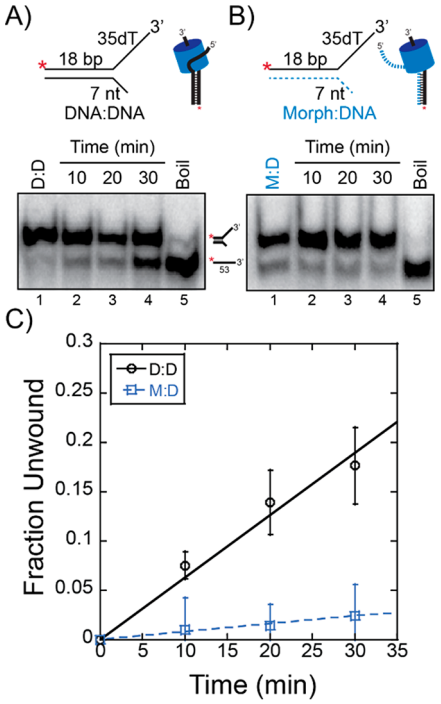

Figure 6. Unwinding of morpholino or DNA forked substrates. Representative unwinding time course for 2 μM *Sso*MCM on either an 18 bp (A) DNA161/DNA162 (D:D) or (B) DNA160m/DNA162 (M:D) substrate (15 nM) with a seven-base 5′-excluded strand flap. Single-turnover experiments were initiated with 2 mM ATP and a single-strand trap identical to the radiolabeled strand as described in Experimental Procedures. (C) Averaged unwinding data for D:D (black circles) were plotted and fitted with a linear regression to give a k of 0.0063 ± 0.0001 min^{-1} and for M:D (blue squares) a k of 0.0008 ± 0.0001 min^{-1}. Error bars are the standard error from three independent experiments.

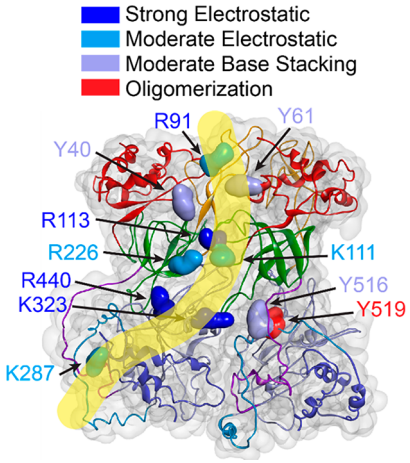

Figure 7. Excluded strand binding path. Structure of the hexameric *Sso*MCM helicase highlighting exterior residues that are influential in binding the excluded strand (yellow). Two of the six subunits are in colored ribbon form with the surface colored gray. Residues are colored and labeled according to the legend for strong (dark blue) or moderate (light blue) electrostatics, moderate base stacking (violet), or the impact on oligomerization (red).

within the CTD domain, which has not been studied previously with regard to structure−function relationships in DNA binding, ATP hydrolysis, or unwinding activity. Overall, this approach enabled us to better define the contributions of the $\alpha/\beta-\alpha$ linker in oligomerization of *Sso*MCM and identified the relative importance of specific external residues that bind the excluded strand to regulate DNA unwinding (Figure 7).

One of the conserved mutations (Y519A) in the $\alpha/\beta-\alpha$ linker had a DNA unwinding and ATPase defect more extreme than all others and correlated with altered global secondary and tertiary structure and hexamer disruption. Previously, residues within *Sso*MCM's NTD and CTD have been implicated in hexamerization.[35] The mutational landscape of *Sso*MCM and the related *Mth*MCM has been studied quite extensively, yet Y519A is one of only two single-point mutations that disrupt the oligomeric state. Previously, multiple mutations were required to disrupt subunit interfaces and change the oligomeric state toward the monomer, including L189D/D191R in the C-subdomain, A416R/A420R in the α/β-region of the CTD, ILI555DSD in the α-region of the CTD, and TPDSP550GGGGG in the α-region of the CTD.[13] The only other single-point mutation that disrupted hexamerization was D488A located at the beginning of the $\alpha/\beta-\alpha$ linker, although DNA binding was not examined.[23] It is interesting to note that unlike Y519A, D488A had increased helicase activity but reduced ATPase activity relative to those of the WT. The induced structural changes for Y519A detected by HDX-MS decreased the rate of DNA unwinding and ATPase activity, although the ATPase activity is stimulated 1.5-fold in the presence of DNA (to the same degree as in the WT). This indicates that the dimer/trimer solution, containing the interfacial subunit ATPase active site,[23,41] can assemble cooperatively in the presence of DNA, but the structural conformations (including hexamerization) required for unwinding are altered.

Y519 appears to reside in a key hydrophobic position within the $\alpha/\beta-\alpha$ linker coordinating packing of V356 (in the α/β-region) on one side and V256 (in the N−C linker) on the other. The Y519A mutation decouples α/β from α and restricts coordination between the NTD and CTD, reducing the degree of communication between the domains. This global structural change can be visualized by our HDX-MS experiments, in which pronounced changes in deuteration uptake are observed locally within the $\alpha/\beta-\alpha$ linker and the CTD and are also propagated through to the NTD. One of the larger increases in the rate of D uptake for Y519 occurs within peptide 109−127, which is within the C-subdomain and normally packs tightly at the interface making the NTD collar. Other regions with increased rates of HDX exchange occur at residues including and surrounding D488 already shown to be important for oligomerization. The rest of the changes in HDX are more difficult to interpret in detail but highlight the expanse of both increases and decreases in the rate of HDX associated with the Y519A mutation that are critical for both oligomeric assembly and controlling communication between the two tiers.

The CD spectrum of Y519A shows a shift of the minima toward 222 nm and a larger negative ellipticity indicating significantly more α-helical character than in the WT. Mutating tyrosine to alanine could extend the $\alpha/\beta-\alpha$ linker helix because of alanine's greater propensity for forming α-helices.[42] Alternatively, the decreased ellipticity for Y519A could be the result of an increased level of secondary structure stabilization for the specific oligomeric states (i.e., dimer or trimer)[43] detected by gel filtration and an EMSA. We note that the positive deviation in ellipticity when Y519A is bound to DNA

DOI: 10.1021/acs.biochem.8b00766
Biochemistry 2018, 57, 5672−5682

is most likely a uniquely altered DNA structure and/or conformation that is induced upon binding of these Y519A specific oligomeric states, as this is not significantly seen with the WT enzyme. Also striking is the apparent increase in α-helical character with temperature noted for Y519A. This profile is harder to explain, because there are few similar examples in the literature, but it seems to indicate an increase in the level of and stabilization of secondary structure with an increase in temperature. We note that the apparent ellipticity (θ_{222}) minimum occurs at 66 °C, which is close to the physiological temperature for *Sso*.

Although gel filtration for Y519A indicates primarily a dimer/trimer/tetramer equilibrium, the EMSA better informs how WT *Sso*MCM is assembled onto DNA. The identification of Y519A dimer and tetramer DNA species in addition to WT trimer and hexamer species allows us to hypothesize about the assembly mechanism on DNA. For Y519A, tighter overall binding is stimulated by a greater equilibrium population of dimer *Sso*MCM complexes that can more easily bind to, engage with, and assemble around DNA stimulating a trimer-of-dimers assembly mechanism. The assembly mechanism appears to be different for the WT, in which transient equilibrium trimeric complexes bind DNA and cooperatively assemble into hexamers in a dimer-of-trimers mechanism. In support of that conclusion, we have already shown that MCM subunits can dynamically exchange freely in solution and when bound to DNA.[2]

Both electrostatic and base-stacking interactions are influential in modulating the binding of the excluded strand to the exterior surface of *Sso*MCM (Figure 7). Some of the strongest effects are observed for mutants around the waist (between the N- and C-terminal domains) and near the top of the N-terminal domain; however, there are contributions to binding the excluded strand all along the lateral length of the hexamer. Thus, the exterior surface path that interacts with the excluded strand exhibits the character of an evolved DNA specific binding domain. It is always possible that these amino acid substitutions may introduce unintentional conformational changes in the hexamer that alter activity. However, excluded strand morpholino substrates that eliminate charge on the DNA effectually reduce DNA unwinding activity by WT *Sso*MCM analogous to the mutated enzymes. Therefore, binding of the excluded strand to the exterior of *Sso*MCM is required for efficient unwinding of DNA duplexes by sequestering and stabilizing the excluded strand to promote forward translocation on the encircled strand.[1,44] Altogether, we have shown that the interaction between the excluded strand and the exterior of *Sso*MCM is both specific and functional. It will be interesting to test whether initial loading of *Sso*MCM on dsDNA replication origins, the transition to encircling a single strand, and activation of unwinding also require interaction of DNA with the exterior of the hexamer. Determining whether the heterohexameric eukaryotic MCM2−7 complex (with six individual subunits) has specific or equivalent preferences for interacting with the excluded strand will require innovative biophysical and structural characterization.

■ ASSOCIATED CONTENT

Supporting Information

The Supporting Information is available free of charge on the ACS Publications website at DOI: 10.1021/acs.biochem.8b00766.

DNA sequences (Table S1) and ATPase hydrolysis rates (Figure S1) (PDF)

■ AUTHOR INFORMATION

Corresponding Author

*One Bear Place #97348, Waco, TX 76798-7348. Telephone: 254-710-2581. E-mail: michael_trakselis@baylor.edu.

ORCID

Nicolas L. Young: 0000-0002-3323-2815
Alan G. Marshall: 0000-0001-9375-2532
Michael A. Trakselis: 0000-0001-7054-8475

Present Address

#B.W.G.: Department of Biological Sciences, University of Pittsburgh, Pittsburgh, PA 15260.

Author Contributions

B.W.G. and M.A.T. designed the experiments. B.W.G., K.L.D., C.T.T., and D.O. performed cloning, prepared the proteins, and performed binding and activity assays. M.E.B. performed unwinding assays with morpholinos. N.L.Y., A.G.M., and M.A.T. designed the HDX-MS experiments that were performed by Y.T. M.A.T. and B.W.G. wrote the manuscript.

Funding

Financial support is provided by Baylor University, a Baylor B-TRUE summer research fellowship (M.E.B.), a Research Scholar Grant (RSG-11-049-01-DMC to M.A.T.) from the American Cancer Society, NSF-MCB (NSF1613534 to M.A.T.), and NSF-DMR (DMR-11-57490 to A.G.M.).

Notes

The authors declare no competing financial interest.

■ ACKNOWLEDGMENTS

The authors thank Conor Haney and W. Seth Horne for providing assistance and access to the Olis CD spectrometer. HDX experiments were performed at the National High Magnetic Field Laboratory. The authors thank the Molecular Bioscience Center (MBC) at Baylor University for access to equipment related to this work. The authors thank Sean Carney, Anthony LaCava, Shiva Gomathinayagam, and Himasha Perera for helpful conversations.

■ ABBREVIATIONS

AAA$^+$, ATPases associated with a variety of activities; ARDD, average relative deuterium uptake difference; CD, circular dichroism; CMG, Cdc45−MCM−GINS complex; CTD, C-terminal domain; dsDNA, double-stranded DNA; EMSA, electrophoretic mobility shift assay; FT-ICR, Fourier transform ion cyclotron resonance; HDX-MS, hydrogen/deuterium exchange mass spectrometry; K_d, dissociation constant; LC, liquid chromatography; MCM, minichromosomal maintenance; *Mth*, *M. thermoautotrophicus*; NHP, N-terminal β-hairpin; NTD, N-terminal domain; *Pfu*, *P. furiosus*; SE, steric exclusion; SEW, steric exclusion and wrapping; ssDNA, single-stranded DNA; *Sso*, *S. solfataricus*; T_m, melting temperature; WT, wild type.

■ REFERENCES

(1) Graham, B. W., Tao, Y., Dodge, K. L., Thaxton, C. T., Olaso, D., Young, N. L., Marshall, A. G., and Trakselis, M. A. (2016) DNA interactions probed by hydrogen-deuterium exchange (HDX) fourier transform ion cyclotron resonance mass spectrometry confirm

DOI: 10.1021/acs.biochem.8b00766
Biochemistry 2018, 57, 5672−5682

external binding sites on the minichromosomal maintenance (MCM) helicase. *J. Biol. Chem. 291*, 12467−12480.
(2) Graham, B. W., Schauer, G. D., Leuba, S. H., and Trakselis, M. A. (2011) Steric exclusion and wrapping of the excluded DNA strand occurs along discrete external binding paths during MCM helicase unwinding. *Nucleic Acids Res. 39*, 6585−6595.
(3) Carney, S. M., Gomathinayagam, S., Leuba, S. H., and Trakselis, M. A. (2017) Bacterial DnaB helicase interacts with the excluded strand to regulate unwinding. *J. Biol. Chem. 292*, 19001−19012.
(4) Slaymaker, I. M., and Chen, X. S. (2012) MCM structure and mechanics: What we have learned from archaeal MCM. *Subcell. Biochem. 62*, 89−111.
(5) Beattie, T. R., and Bell, S. D. (2011) Molecular machines in archaeal DNA replication. *Curr. Opin. Chem. Biol. 15*, 614−619.
(6) Brewster, A. S., and Chen, X. S. (2010) Insights into the MCM functional mechanism: lessons learned from the archaeal MCM complex. *Crit. Rev. Biochem. Mol. Biol. 45*, 243−256.
(7) Yoshimochi, T., Fujikane, R., Kawanami, M., Matsunaga, F., and Ishino, Y. (2008) The GINS complex from *Pyrococcus furiosus* stimulates the MCM helicase activity. *J. Biol. Chem. 283*, 1601−1609.
(8) Froelich, C. A., Kang, S., Epling, L. B., Bell, S. P., and Enemark, E. J. (2014) A conserved MCM single-stranded DNA binding element is essential for replication initiation. *eLife 3*, e01993.
(9) Marinsek, N., Barry, E. R., Makarova, K. S., Dionne, I., Koonin, E. V., and Bell, S. D. (2006) GINS, a central nexus in the archaeal DNA replication fork. *EMBO Rep. 7*, 539−545.
(10) Lang, S., and Huang, L. (2015) *Sulfolobus* GINS complex stimulates DNA binding and processive DNA unwinding by MCM. *J. Bacteriol. 197*, 3409−3420.
(11) Costa, A., Renault, L., Swuec, P., Petojevic, T., Pesavento, J. J., Ilves, I., MacLellan-Gibson, K., Fleck, R. A., Botchan, M. R., and Berger, J. M. (2014) DNA binding polarity, dimerization, and ATPase ring remodeling in the CMG helicase of the eukaryotic replisome. *eLife 3*, e03273.
(12) Moyer, S. E., Lewis, P. W., and Botchan, M. R. (2006) Isolation of the Cdc45/Mcm2−7/GINS (CMG) complex, a candidate for the eukaryotic DNA replication fork helicase. *Proc. Natl. Acad. Sci. U. S. A. 103*, 10236−10241.
(13) Brewster, A. S., Wang, G., Yu, X., Greenleaf, W. B., Carazo, J. M., Tjajadi, M., Klein, M. G., and Chen, X. S. (2008) Crystal structure of a near-full-length archaeal MCM: Functional insights for an AAA^+ hexameric helicase. *Proc. Natl. Acad. Sci. U. S. A. 105*, 20191−20196.
(14) Slaymaker, I. M., Fu, Y., Toso, D. B., Ranatunga, N., Brewster, A., Forsburg, S. L., Zhou, Z. H., and Chen, X. S. (2013) Mini-chromosome maintenance complexes form a filament to remodel DNA structure and topology. *Nucleic Acids Res. 41*, 3446−3456.
(15) Fu, Y., Slaymaker, I. M., Wang, J., Wang, G., and Chen, X. S. (2014) The 1.8-A crystal structure of the N-terminal domain of an archaeal MCM as a right-handed filament. *J. Mol. Biol. 426*, 1512−1523.
(16) Miller, J. M., Arachea, B. T., Epling, L. B., and Enemark, E. J. (2014) Analysis of the crystal structure of an active MCM hexamer. *eLife 3*, e03433.
(17) Pape, T., Meka, H., Chen, S., Vicentini, G., van Heel, M., and Onesti, S. (2003) Hexameric ring structure of the full-length archaeal MCM protein complex. *EMBO Rep. 4*, 1079−1083.
(18) Chen, Y. J., Yu, X., Kasiviswanathan, R., Shin, J. H., Kelman, Z., and Egelman, E. H. (2005) Structural polymorphism of *Methanothermobacter thermautotrophicus* MCM. *J. Mol. Biol. 346*, 389−394.
(19) Gomez-Llorente, Y., Fletcher, R. J., Chen, X. S., Carazo, J. M., and San Martín, C. (2005) Polymorphism and double hexamer structure in the archaeal minichromosome maintenance (MCM) helicase from *Methanobacterium thermoautotrophicum*. *J. Biol. Chem. 280*, 40909−40915.
(20) Yu, X., VanLoock, M. S., Poplawski, A., Kelman, Z., Xiang, T., Tye, B. K., and Egelman, E. H. (2002) The *Methanobacterium thermoautotrophicum* MCM protein can form heptameric rings. *EMBO Rep. 3*, 792−797.
(21) Samson, R. Y., and Bell, S. D. (2016) Archaeal DNA Replication Origins and Recruitment of the MCM Replicative Helicase. *Enzymes 39*, 169−190.
(22) McGeoch, A. T., Trakselis, M. A., Laskey, R. A., and Bell, S. D. (2005) Organization of the archaeal MCM complex on DNA and implications for the helicase mechanism. *Nat. Struct. Mol. Biol. 12*, 756−762.
(23) Moreau, M. J., McGeoch, A. T., Lowe, A. R., Itzhaki, L. S., and Bell, S. D. (2007) ATPase site architecture and helicase mechanism of an archaeal MCM. *Mol. Cell 28*, 304−314.
(24) Wiedemann, C., Szambowska, A., Hafner, S., Ohlenschlager, O., Guhrs, K. H., and Gorlach, M. (2015) Structure and regulatory role of the C-terminal winged helix domain of the archaeal minichromosome maintenance complex. *Nucleic Acids Res. 43*, 2958−2967.
(25) Bauer, R. J., Wolff, I. D., Zuo, X., Lin, H. K., and Trakselis, M. A. (2013) Assembly and distributive action of an archaeal DNA polymerase holoenzyme. *J. Mol. Biol. 425*, 4820−4836.
(26) Bauer, R. J., Graham, B. W., and Trakselis, M. A. (2013) Novel interaction of the bacterial-Like DnaG primase with the MCM helicase in archaea. *J. Mol. Biol. 425*, 1259−1273.
(27) Bauer, R. J., Begley, M. T., and Trakselis, M. A. (2012) Kinetics and fidelity of polymerization by DNA polymerase III from *Sulfolobus solfataricus*. *Biochemistry 51*, 1996−2007.
(28) Perez-Iratxeta, C., and Andrade-Navarro, M. A. (2008) K2D2: Estimation of protein secondary structure from circular dichroism spectra. *BMC Struct. Biol. 8*, 25.
(29) Andrade, M. A., Chacon, P., Merelo, J. J., and Moran, F. (1993) Evaluation of secondary structure of proteins from UV circular dichroism spectra using an unsupervised learning neural network. *Protein Eng., Des. Sel. 6*, 383−390.
(30) Greenfield, N. J. (2007) Using circular dichroism spectra to estimate protein secondary structure. *Nat. Protoc. 1*, 2876−2890.
(31) Blakney, G. T., Hendrickson, C. L., and Marshall, A. G. (2011) Predator data station: A fast data acquisition system for advanced FT-ICR MS experiments. *Int. J. Mass Spectrom. 306*, 246−252.
(32) Zhang, Z., Li, W., Logan, T. M., Li, M., and Marshall, A. G. (1997) Human recombinant [C22A] FK506-binding protein amide hydrogen exchange rates from mass spectrometry match and extend those from NMR. *Protein Sci. 6*, 2203−2217.
(33) Zhang, Q., Willison, L. N., Tripathi, P., Sathe, S. K., Roux, K. H., Emmett, M. R., Blakney, G. T., Zhang, H. M., and Marshall, A. G. (2011) Epitope mapping of a 95 kDa antigen in complex with antibody by solution-phase amide backbone hydrogen/deuterium exchange monitored by Fourier transform ion cyclotron resonance mass spectrometry. *Anal. Chem. 83*, 7129−7136.
(34) Bou-Assaf, G. M., and Marshall, A. G. (2015) Chapter 12: Biophysical Mass Spectrometry for Biopharmaceutical Process Development: Focus on Hydrogen/Deuterium Exchange. In *Biophysical Characterization of Proteins in Developing Biopharmaceuticals* (Berkowitz, D. J. H. A., Ed.) pp 307−339, Elsevier, Amsterdam.
(35) Barry, E. R., McGeoch, A. T., Kelman, Z., and Bell, S. D. (2007) Archaeal MCM has separable processivity, substrate choice and helicase domains. *Nucleic Acids Res. 35*, 988−998.
(36) Golbik, R., Zahn, R., Harding, S. E., and Fersht, A. R. (1998) Thermodynamic stability and folding of GroEL minichaperones. *J. Mol. Biol. 276*, 505−515.
(37) Buchan, D. W., Minneci, F., Nugent, T. C., Bryson, K., and Jones, D. T. (2013) Scalable web services for the PSIPRED Protein Analysis Workbench. *Nucleic Acids Res. 41*, W349−357.
(38) Summerton, J., and Weller, D. (1997) Morpholino antisense oligomers: Design, preparation, and properties. *Antisense Nucleic Acid Drug Dev. 7*, 187−195.
(39) Tackett, A. J., Wei, L., Cameron, C. E., and Raney, K. D. (2001) Unwinding of nucleic acids by HCV NS3 helicase is sensitive to the structure of the duplex. *Nucleic Acids Res. 29*, 565−572.
(40) Garaycoechea, J. I., and Patel, K. J. (2014) Why does the bone marrow fail in Fanconi anemia? *Blood 123*, 26−34.

DOI: 10.1021/acs.biochem.8b00766
Biochemistry 2018, 57, 5672−5682

(41) Liew, L. P., and Bell, S. D. (2011) The interplay of DNA binding, ATP hydrolysis and helicase activities of the archaeal MCM helicase. *Biochem. J. 436*, 409−414.
(42) Pace, C. N., and Scholtz, J. M. (1998) A helix propensity scale based on experimental studies of peptides and proteins. *Biophys. J. 75*, 422−427.
(43) Hennessey, J. P., Jr., Johnson, W. C., Jr., Bahler, C., and Wood, H. G. (1982) Subunit interactions of transcarboxylase as studied by circular dichroism. *Biochemistry 21*, 642−646.
(44) Carney, S. M., and Trakselis, M. A. (2016) The excluded DNA strand is SEW important for hexameric helicase unwinding. *Methods 108*, 79−91.

DOI: 10.1021/acs.biochem.8b00766
Biochemistry 2018, 57, 5672−5682